



# Historical Biology

## An International Journal of Paleobiology



ISSN: (Print) (Online) Journal homepage: <https://www.tandfonline.com/loi/ghbi20>

# A new morphotype of nothosaurs (Sauropterygia: Nothosauridae) from the Middle Triassic of South China

Yi-Wei Hu & Jun Liu

To cite this article: Yi-Wei Hu & Jun Liu (2022): A new morphotype of nothosaurs (Sauropterygia: Nothosauridae) from the Middle Triassic of South China, *Historical Biology*, DOI: [10.1080/08912963.2022.2122459](https://doi.org/10.1080/08912963.2022.2122459)

To link to this article: <https://doi.org/10.1080/08912963.2022.2122459>



Published online: 12 Sep 2022.



Submit your article to this journal



View related articles



View Crossmark data



# A new morphotype of nothosaurs (Sauropterygia: Nothosauridae) from the Middle Triassic of South China

Yi-Wei Hu and Jun Liu

Division of Geology, School of Resources and Environmental Engineering, Hefei University of Technology, Hefei, China

## ABSTRACT

A new morphotype of nothosaurs collected from the Upper Member of Anisian Guanling Formation in the Muta village, Luxi County, Yunnan Province, China is reported here. The new morphotype is represented by a single specimen that can be distinguished from other nothosaurs in the combination of the following features: premaxilla partly fused, jugal positioned forward in the cheek, pineal foramen in a deep trough and close to the middle of the skull table, quadratojugal present, distinctly long internal naris. The right lower jaw of the new specimen is completely exposed in medial view, providing hereto unknown information about the medial morphology of the lower jaw for nothosaurid sauropterygians, including the large splenial forming half of the inner wall of the lower jaw, the slender and elongate coronoid located in the middle of the mandible, and the Meckelian foramen located within the adductor fossa bounded by surangular and prearticular. Morphological comparison with other Triassic eosaurophterygians reveals previously unrecognised characters that may be used for reconstructing the phylogeny of sauropterygians in the future.

## ARTICLE HISTORY

Received 21 July 2022

Accepted 4 September 2022

## KEYWORDS

Nothosaurus; Lariosaurus;  
Permo-Triassic Mass  
Extinction; marine reptiles

## Introduction

After the devastating Permo-Triassic Mass Extinction, several new groups of large predators invaded the sea in the early part of the Triassic, including sauropterygians, ichthyosauromorphs and thalattosaurs (Scheyer et al. 2014; Kelley and Pyenson 2015; Motani et al. 2015; Stubbs and Benton 2016; Li and Liu 2020; Sander et al. 2021). Among these predators, sauropterygians are the most abundant group in terms of the generic/species diversity (Rieppel 2000; Benson et al. 2010; Motani and Vermeij 2021). They originated in the Early Triassic (Li and Liu 2020), and played a major role in the Mesozoic oceanic ecosystem since then until their extinction at the end of the Cretaceous (Motani 2009).

Nothosauridae is a very speciose family of sauropterygians. It traditionally consists of *Nothosaurus* and *Lariosaurus* (Rieppel 2000), and includes 20 valid species as currently recognised (Liu et al. 2014; Hinz et al. 2019; Li and Liu 2020; Lin et al. 2021). The research of nothosaurid sauropterygians can go back to Meyer (1847:55) when he described *Nothosaurus* and *Placodus* from the Germanic Muschelkalk beds in monumental Fauna der Vorwelt ('fauna of the ancient world'). Unsurprisingly, most studies about nothosaurs were conducted in Europe, and the differentiation of *Nothosaurus* and *Lariosaurus* was mostly based on the study of European nothosaurs, especially in the skull region (Rieppel 2000). With the discovery of several now-famous marine Triassic faunas found in South China (Benton et al. 2013), many new nothosaurids were also published from the eastern part of the Tethys ocean. These include *Lariosaurus xingyiensis* (Lin et al. 2017), *L. hongguoensis* (Jiang et al. 2006a), *L. sanxiaensis* (Li and Liu 2020), *Nothosaurus yangtzeensis* (Yin et al. 2014), and *N. youngi* (Ji et al. 2014). The discovery of Chinese nothosaurs blurred the formerly recognised distinction between *Nothosaurus* and *Lariosaurus* (Liu et al. 2014; Lin et al. 2017) and consequently, phylogenetic relationships of nothosaurs have been in urgent need for revision (Liu et al. 2014; Klein et al. 2016; Li and Liu 2020; Lin

et al. 2021). The best way to resolve conflicting phylogenetic hypothesis is the sampling of new taxa and the discovery of more informative characters (Rieppel et al. 2002; Li and Liu 2020; Lin et al. 2021).

Although many skulls of Nothosauridae, especially those from the western Tethys, have been described in detail (see the review in Rieppel 2000), little is known about the medial morphology of the lower jaw in Nothosauridae. Hitherto, the morphology of the lower jaw of Nothosauridae in medial view has been rarely described, except in one case where the posterior part of the lower jaw of a *Nothosaurus* specimen has been figured (Rieppel 1994). Even among eosaurophterygians, only few taxa provided morphological information regarding the lower jaw in medial view, such as *Neusticosaurus pusillus* (Sander 1989), *Simosaurus gaillardotii* (Rieppel 1994) and *Anarosaurus heterodontus* (Klein 2009).

In this paper, we describe the detailed morphology of a new morphotype of Nothosauridae from southwest China. The new morphotype is represented by a single specimen collected from the Upper Member of the Anisian Guanling Formation in the Muta village, Luxi County, Yunnan Province, China. The complete medial wall of the lower jaw and part of the otic capsule is exposed, providing hereto unknown information about the morphology of nothosaurid sauropterygians.

## Material and methods

The new specimen was collected from an abandoned quarry (E103° 55'55.52", N24°31'6.57") in Muta village, Luxi County, Yunnan Province by the local amateur palaeontologist S.P. Jiang collected this specimen in 2018. It was donated and transferred to the Geological Museum of Hefei University of Technology (HFUT) in 2019 and is now stored there under the collection number HFUT LX-19-001. Geological mapping in the region (Figure 1) indicates that the stratum generating the specimen is from the Upper

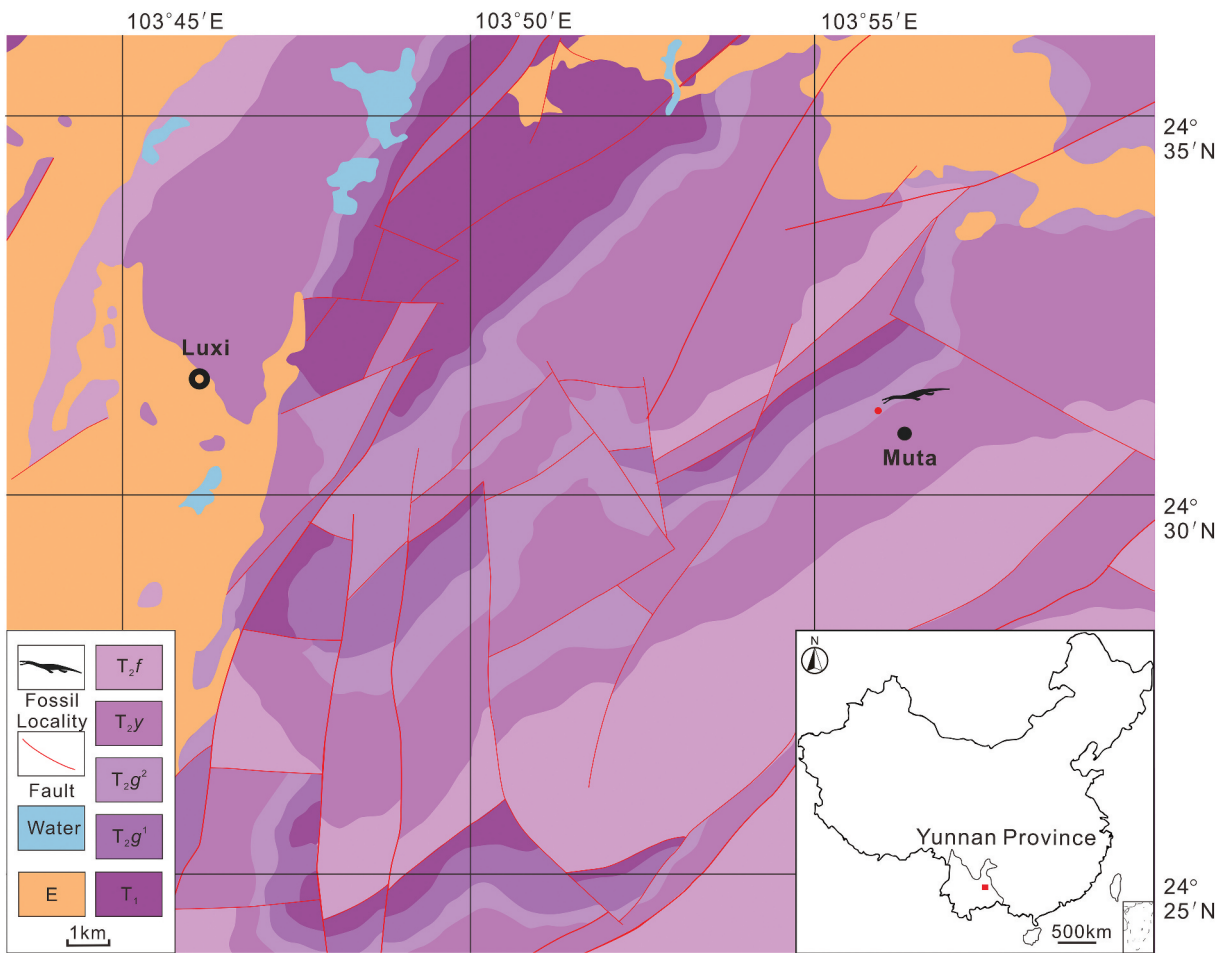


**Figure 1.** The geologic map showing the quarry where HFUT LX-19-001 was discovered (updated after YBGMR (Yunnan Bureau of Geology and Mineral Resources) 1990). Inset is a Chinese map. Abbreviations: E, Palaeogene; T<sub>2</sub>f, Falang Formation, Ladinian, Middle Triassic; T<sub>2</sub>y, Yangliujing Formation, Anisian-Ladinian, Middle Triassic; T<sub>2</sub>g<sup>2</sup>, Upper Member of Guanling Formation, Anisian, Middle Triassic; T<sub>2</sub>g<sup>1</sup>, Lower Member of Guanling Formation, Anisian, Middle Triassic; T<sub>1</sub>, Lower Triassic.

Member of the Anisian Guanling Formation, formerly known as Gejiu Formation in YBGMR (Yunnan Bureau of Geology and Mineral Resources) (1990). The new specimen was prepared from both sides with pneumatic tools and needles. The pictures were taken using a NIKON D7200 camera and the measured data were collected using a digital caliper with 0.01 mm precision.

### Systematic palaeontology

#### Sauroptrygia Owen 1860

##### Eosauropterygia Rieppel 1994

##### Nothosauroidea Baur 1889

##### Nothosauridae Baur 1889

Nothosauridae indet.

### Material

HFUT LX-19-001, a complete skull with part of the cervical exposed in dorsolateral view (Figure 2; Table 1).

### Horizon

Upper Member of Guanling Formation, Anisian, Middle Triassic.

### Locality

Muta village, Luxi County, Yunnan Province, China.

### Description

The new specimen is an incomplete skeleton preserving the entire skull and 20 cervical vertebrae. The whole specimen is largely exposed in lateral view (Figure 2). Calcite veins cut across the specimen in several places.

### The skull

The skull was prepared from both sides (Figure 3). The region of the upper temporal fenestra of the left skull experienced some crush. Otherwise, the skull is well preserved with a condylobasal length of 147.8 mm.

The premaxillae are fused in the anterior part, forming the short and blunt rostrum. Its surface is sculptured with some small pits. The region where premaxillae contact nasals is broken, but the premaxilla is definitely separated from the frontal. The rostrum is distinctly constricted behind the premaxilla-maxilla suture.

The maxilla is a long bone with the posterior process extending posteriorly to a level beyond the posterior corner of the orbit. It forms the entire lateral margin of the external naris and also



**Figure 2.** HFUT LX-19-001 in dorsolateral view. Scale bar equals 10 cm.

**Table 1.** Measurements of HFUT LX-19-001.

Measurement	Value (mm)
Distance from tip of snout to occipital condyle	147.8
Distance from tip of snout to anterior margin of external naris	25.6
Distance from tip of snout to anterior margin of orbital	52.3
Distance from tip of snout to anterior margin of upper temporal fenestra	90.2
Distance from posterior margin of external naris to anterior margin of orbital	9.5
Distance from posterior margin of orbital to anterior margin of upper temporal fenestra	4.1
Longitudinal diameter of external naris	15.2
Transverse diameter of external naris	5.5
Longitudinal diameter of orbital	32.7
Transverse diameter of orbital	20.1
Longitudinal diameter of upper temporal fenestra	49.2
Transverse diameter of upper temporal fenestra	10.2
Length of retroarticular process	20.8
Length of mandibular symphysis	20.7

contributes to a significant part of the lateral margin of the orbit. Anteriorly, the maxilla meets the premaxilla at the level of the anterior corner of the external naris in a curved suture. In the antorbital region, the dorsal process of the maxilla enters between

the prefrontal and the nasal, and contacts the frontal posterodorsally. Posteriorly, the maxilla extends back to contact the jugal and postorbital.

The paired nasals are slender. The suture between the nasal and premaxilla is blurred by a break in the region, but the nasal must form most of the dorsal margin of the external naris, if not all. The nasal sends the process backward along the midline separating the anterolateral processes of the frontal, almost reaching the anterior orbit margin.

The prefrontal is a crescent-shaped bone that forms the entire anterior border of the orbit. Anteriorly, it separates the maxilla and orbit by a marked ridge. Posterodorsally, the prefrontal contacts the frontal and sends a process along the dorsal margin of the orbit, which terminates at a point at one-third length of the orbit backward.

The partly paired frontals are twice as long as nasals, forming the entire interorbital skull roof. The anterolateral process of the frontal intrudes between the nasal and maxilla. Posteriorly, the location of the serrated suture of the frontal with parietal is at a level just behind the anterior corner of the temporal fenestra.

The postfrontal is subtriangular and constitutes the posterodorsal margin of the orbit. Dorsally, it meets the frontal. Laterally, the postfrontal-postorbital suture is a serrated line. Posteriorly, the

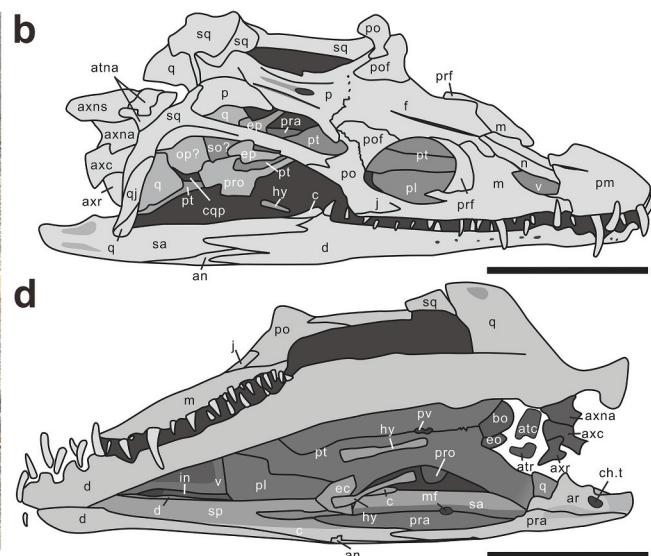
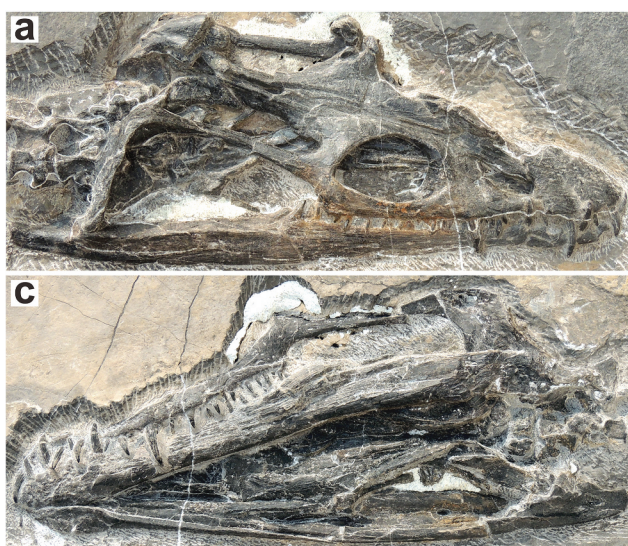


**Figure 3.** Skull of HFUT LX-19-001. (a) Photo showing the dorsolateral view of the skull; (b) Interpretative drawing of (a); (c) Photo showing the ventrolateral view of the skull; (d) Interpretative drawing of (c). Abbreviations: an, angular; ar, articular; atc, atlas centrum; atna, atlas neural arch; atr, atlas rib; axc, axis centrum; axna, axis neural arch; axns, axis neural spine; axr, axis rib; bo, basioccipital; c, coronoid; ch.t, chorda tympani foramen; cqp, cranoquadrate passage; d, dentary; ec, ectopterygoid; eo, exoccipital; ep, epipterygoid; f, frontal; hy, hyoid; j, jugal; in, internal naris; m, maxilla; mf, Meckelian foramen; n, nasal; op, opisthotic; p, parietal; pl, palatine; pm, premaxilla; po, postorbital; pof, postfrontal; pra, prearticular; prf, prefrontal; pro, prootic; pt, pterygoid; pv, palatine vacuity; q, quadrate; qj, quadrojugal; sa, surangular; so, supraoccipital; sp, splenial; sq, squamosal; v, vomer. Scale bars equal 5 cm.

posterior process of the postfrontal marginally contacts the parietal. The postfrontal is excluded from the upper temporal fenestra by the contact of the parietal and postorbital.

The postorbital constitutes the entire anterior corner of the upper temporal fenestra. Anteriorly, the postorbital meets the jugal and maxilla below the orbit. The posterior process of the postorbital is short, meeting the squamosal with an interdigitating suture. The surface of the postorbital has a distinct radial sculpture.

The jugal is a small bone. Because the suture between the jugal and postorbital is unclear on both sides of the skull, whether or not the jugal enters the orbit is uncertain. As it can be seen from the right side of the skull, the anterior end of the jugal is close to the midpoint of the orbit. On the left side of the skull, the jugal meets the anterior process of the postorbital and contacts the maxilla laterally. It is clear that the jugal is excluded from the upper temporal arch.

The parietals are fused. The pineal foramen is located in the anterior end of a deep trough. The anterolateral process of the parietal separates the frontal and postfrontal from the upper temporal fenestra. The parietal skull table is strongly constricted, and there is no constriction behind the pineal foramen. Posterolaterally, the parietal contacts the squamosal. However, the suture line was destroyed due to the crush in the region.

The squamosal is a large triradiate bone, defining almost the entire lateral margin of the upper temporal fenestra. The lateral process of the squamosal is separated from the ventral margin of the skull broadly, and meets the quadrate and quadratojugal. Its anterior process contacts the postorbital and forms the majority of the temporal arch.

The quadratojugal can be only observed on the right side of the skull due to preservation. It forms a bulge and sheathes the quadrate.

The quadrate is barely exposed in lateral view because the quadratojugal largely covers the quadrate dorsolaterally. In the anterolateral view, it is clearly seen that the quadrate caps the quadrate ramus of the pterygoid. The ventral view of the skull reveals that the left quadrate forms the posterior margin of the lower temporal embayment.

The epitylgoid can be clearly identified on the right side of the skull. Ventrally, the epitylgoid has a broad base sutured to the pterygoid. The anterior process extends to below the squamosal. The posterior part of the base contacts the prootic laterally and supraoccipital posteriorly. There is a large cleft between the epitylgoid and prootic. Dorsally, the epitylgoid becomes narrower and overlaps the descensus squamosal laterally. Due to the postmortem deformation, the epitylgoid shows no contact with the parietal.

One of the otic capsule elements, the prootic, can be confidently identified on the right side of the skull. The anterior process of the prootic is covered by the upper temporal arch, forming a well-developed ridge. The posterolateral margin of the base of prootic shows a distinct inverted V-shape, hosting the exit of the facial nerve (nerve VII). In ventral view, the prootic forms a rounded process laterally. Posteriorly, the opening of the cranioquadrate passage is behind the prootic and bounded by the quadrate ramus of pterygoid ventrally and opisthotic dorsally. No sign of stapes can be observed.

The supraoccipital, if correctly identified, has a distinct sagittal crest in dorsal view and contacts the opisthotic laterally. The basioccipital only exposes the posterior part in ventral view.

In ventral view, the left palate is mostly covered by the lower jaw, but the right palate is well exposed. Nonetheless, the anterior part of the palate is damaged due to compaction. Thus, the sutures between vomer, palatine and pterygoid are difficult to be delineated with

confidence. However, the internal naris appears to be distinctly long, one of the autapomorphies of the taxon compared with other nothosaurids. The paired pterygoids occupy the most of the exposed palate. The transverse process of the pterygoid is well developed and longitudinally oriented. Near the posterior end of the palate, there is an opening, which is similar to the 'posterior interpterygoid vacuity' described in *Diandongosaurus acutidentatus* (Sato et al. 2014; Liu et al. 2015). However, this opening is different from the posterior interpterygoid vacuity present in pistosaurs, which is quite large and exposes the basisphenoid and parasphenoid (e.g., Rieppel et al. 2002; Sato et al. 2010). Posteriorly, the terminal quadrate ramus of the pterygoid is embraced by the quadrate. Two hyoids are well preserved, but both are dislocated. The hyoid is slender and slightly expanded at both ends. The ectopterygoid is a subtriangular element contacting the pterygoid laterally and the palatine anteriorly. The pterygoid flange is indistinct.

### **Lower jaw**

Although the posterior part of the left lower jaw was damaged due to the taphonomic compaction, the right lower jaw is well-preserved and completely prepared in both lateral and medial views. The lower jaw has a well-developed retroarticular process, built laterally by the surangular and medially by the articular and prearticular.

In ventral view, the mandibular symphysis is unfused and elongated. The posterior part of the lower jaw hosts a large adductor fossa that is bounded anteriorly by the splenial, laterally by the surangular and prearticular, and ventrally by the prearticular. Within the adductor fossa, the oval Meckelian foramen is embraced entirely by the surangular and prearticular.

The dentary covers about three-fourths of the lateral surface of the lower jaw, with distinct longitudinal sculpturing. A series of small pits run longitudinally, passing the alveolar nerve and vessels (Benton and Westoll 1983; Sander 1989). Posteriorly, the dentary has two processes. One of them interfingers with the surangular and the other with the angular. In medial view, the dentary embraces the splenial.

The splenial is only visible in medial view. It forms the anterior wall of the lower jaw and enters the mandibular symphysis anteriorly. Posteriorly, the splenial divides into two branches that embrace the coronoid and prearticular.

The coronoid is a slender and elongated bone. In lateral view, an obvious coronoid process is present immediately behind the last dentary tooth. In medial view, part of the bone is covered by the dislocated ectopterygoid and hyoid. Anteriorly, the coronoid wedges into the splenial. Posteriorly, it contacts the surangular. The coronoid forms the anterior margin of the adductor fossa.

The exposed angular is a small bone. In lateral view, the angular contacts the surangular dorsally and interdigitates with the dentary anteriorly. In medial view, it is located ventral to the dentary and prearticular.

The surangular is the second-largest bone in the lower jaw, only smaller than the dentary. In lateral view, the anterior process runs between the coronoid and dentary. Posteriorly, it forms the entire lateral wall of the retroarticular process and glenoid fossa. A distinct trough on the lateral surface of the retroarticular process is present, comprising the insertion area for the mandibulae muscle. In medial view, the surangular is bounded by the coronoid anteriorly and the prearticular ventrally. A distinct flange for the insertion of adductor muscle is present on the surangular.

The prearticular is ventral to the surangular and articular, comprising part of the medial and lateral wall of the adductor fossa. The anterior process of the prearticular is embraced by the splenial and

coronoid. Posteriorly, the prearticular supports the retroarticular process ventral to the articular.

The articular is only exposed in medial view. The articular is bounded ventrally by the prearticular and laterally by the surangular. It forms the saddle-shaped part of the articular facet and the medial wall of the retroarticular process. Below the articular facet, the strong depression on the articular serves as the insertion site for the depressor mandibulae. Behind this, the articular shows a distinct foramen, most likely the chorda tympani foramen through which the facial nerve (nerve VII) enters the lower jaw to provide taste sensation of the tongue.

### Dentition

Judging from the tooth sockets on the premaxilla, there are five upright premaxillary fangs, but only four on the right side and three on the left side can be observed. Two of the four visible premaxillary teeth on the right skull are small, which are presumably replacement teeth.

The maxillary tooth row extends backward to a level at the posterior corner of the orbit. There is only one maxillary fang and three normal maxillary teeth present anterior to the maxillary fang on both sides of the skull. Posterior to the maxillary fang, seven and 11 teeth are preserved on the right and left skull, respectively. Judging from the space between the teeth, there should be more than 11 maxillary teeth posterior to the maxillary fang.

The dentary dentition ends at a level below the anterior corner of the upper temporal fenestra. On the right side, three dentary fangs are preserved and two large tooth sockets can be observed. Therefore, there are five dentary fangs.

### Postcranial skeleton

A total of 20 cervical vertebrae are preserved (Figure 2). The distinct neurocentral suture can be observed in HFUT LX-19-001 (Figure 4). The atlas-axis complex was prepared from both sides (Figure 3). The small atlas centrum is half as long as other vertebral centra. The atlas neural arch is partially covered by the squamosal in lateral view. The atlas rib is a boot-shaped element. The anteroposterior length of the axis centrum is longer than its height, which is similar to the centra behind it, but its neural spine is twice as long as other neural spines. All preserved neural spines are longer than tall. The neural spine of the 3<sup>rd</sup> cervical vertebra is semicircular in shape (Figure 4). Then the neural spine gradually becomes longer and rectangle-shaped. The transverse processes of cervical vertebrae are stubby without expanding towards the end. All cervical ribs are single-headed. The anterior process of cervical ribs is well-developed. Based on the well-developed anterior process of the 19<sup>th</sup> cervical rib, we infer that the number of cervical vertebrae in HFUT LX-19-001 is many more than 20.

### Discussion

#### Ontogenetic evaluation of HFUT LX-19-001

HFUT LX-19-001 only preserved the skull and part of the cervical, which make the evaluation of the ontogenetic stage difficult. However, there are still several morphological features present on the skull being useful in assessing the ontogenetic stage. The dermatocranum of HFUT LX-19-001 is distinctly sculptured and the braincase is well ossified, suggesting that the specimen is not a juvenile. However, the frontal is only partially fused in HFUT LX-19-001, being different from the adult skull of other nothosaurids where the frontals are fully fused (Figure 5). The sutures

between the neural arch and centrum are also clearly visible in HFUT LX-19-001. The combinations of these morphological features suggest that HFUT LX-19-001 is most likely a subadult.

#### Comparison with other nothosaurids from the Middle Triassic of South China

HFUT LX-19-001 shows a lot of clearly derived characters of Nothosauridae, including the elongated rostrum strongly constricted at the level of the external naris, the postorbital forming the entire anterior margin of the enlarged upper temporal fenestra, the reduced prefrontal, and the strongly depressed temporal region. In the Middle Triassic of South China, four species of nothosaurids are currently recognised. These are *Nothosaurus yangtzeensis* (Shang 2006; Jiang 2006b; Yin et al. 2014) and *Lariosaurus hongguoensis* (Jiang et al. 2006a) from the middle Anisian Panxian fauna, and *N. youngi* (Li and Rieppel 2004; Ji et al. 2014) and *L. xingyiensis* (Li et al. 2002; Rieppel et al. 2003; Lin et al. 2017) from the late Ladinian Xingyi fauna. Below we compare HFUT LX-19-001 with all these four Chinese nothosaurids in detail (Figures 5 and 6; Table 2).

***Nothosaurus yangtzeensis*.** – The holotype of *N. yangtzeensis* (GMPKU-P-1080) is a medium-sized *Nothosaurus* with a condylobasal length of 324 mm. It is as twice large as HFUT LX-19-001. The other published specimen (272 mm in GMPKU-P-3014) is also much bigger than HFUT LX-19-001. The ratio of the longitudinal diameter of the upper temporal fenestra to longitudinal diameter of the external naris of *N. yangtzeensis* (5.96 and 4.67, respectively, in the holotype and GMPKU-P-3014) is much more than HFUT LX-19-001 (3.24). In *N. yangtzeensis*, the nasal contacts the prefrontal, but this contact is absent in HFUT LX-19-001. The jugal enters the upper temporal arch and contacts the squamosal in the holotype of *N. yangtzeensis*, which is different from HFUT LX-19-001. In *N. yangtzeensis*, the parietal constricts in the posteriormost part. However, there is no constriction in the posteriormost part of the parietal in HFUT LX-19-001. Finally, *N. yangtzeensis* has four premaxillary fangs and two maxillary fangs, while in HFUT LX-19-001 the number is five and one, respectively.

***Lariosaurus hongguoensis*.** – The holotype of *L. hongguoensis* is a small-sized specimen with a condylobasal length of 80 mm, which is much smaller than HFUT LX-19-001. The interorbital septum of *L. hongguoensis* is much slender than that of HFUT LX-19-001. In addition, there is no coronoid process in *L. hongguoensis*. Also, *L. hongguoensis* has seven premaxillary teeth including five fangs and two small teeth. But HFUT LX-19-001 only has five premaxillary teeth.

***Lariosaurus xingyiensis*.** – *L. xingyiensis* is different from HFUT LX-19-001 in that its jugal is absent, the nasal contacts the prefrontal, and the parietal constricts in the posteriormost part. In addition, the splenial of *L. xingyiensis* is separated from the mandibular symphysis, but the splenial enters the mandibular symphysis in HFUT LX-19-001.

***Nothosaurus youngi*.** – The ratio of the longitudinal diameter of the upper temporal fenestra divided by the longitudinal diameter of the external naris in *N. youngi* is 5.00 (IVPP V 13590) and 4.69 (WS-30-R24), while it is 3.24 in HFUT LX-19-001. The nasal meets the prefrontal posteriorly in *N. youngi*, being different from HFUT LX-19-001. Also, the pineal foramen of *N. youngi* is located in the middle of a trough, but the pineal foramen is displaced towards the anterior

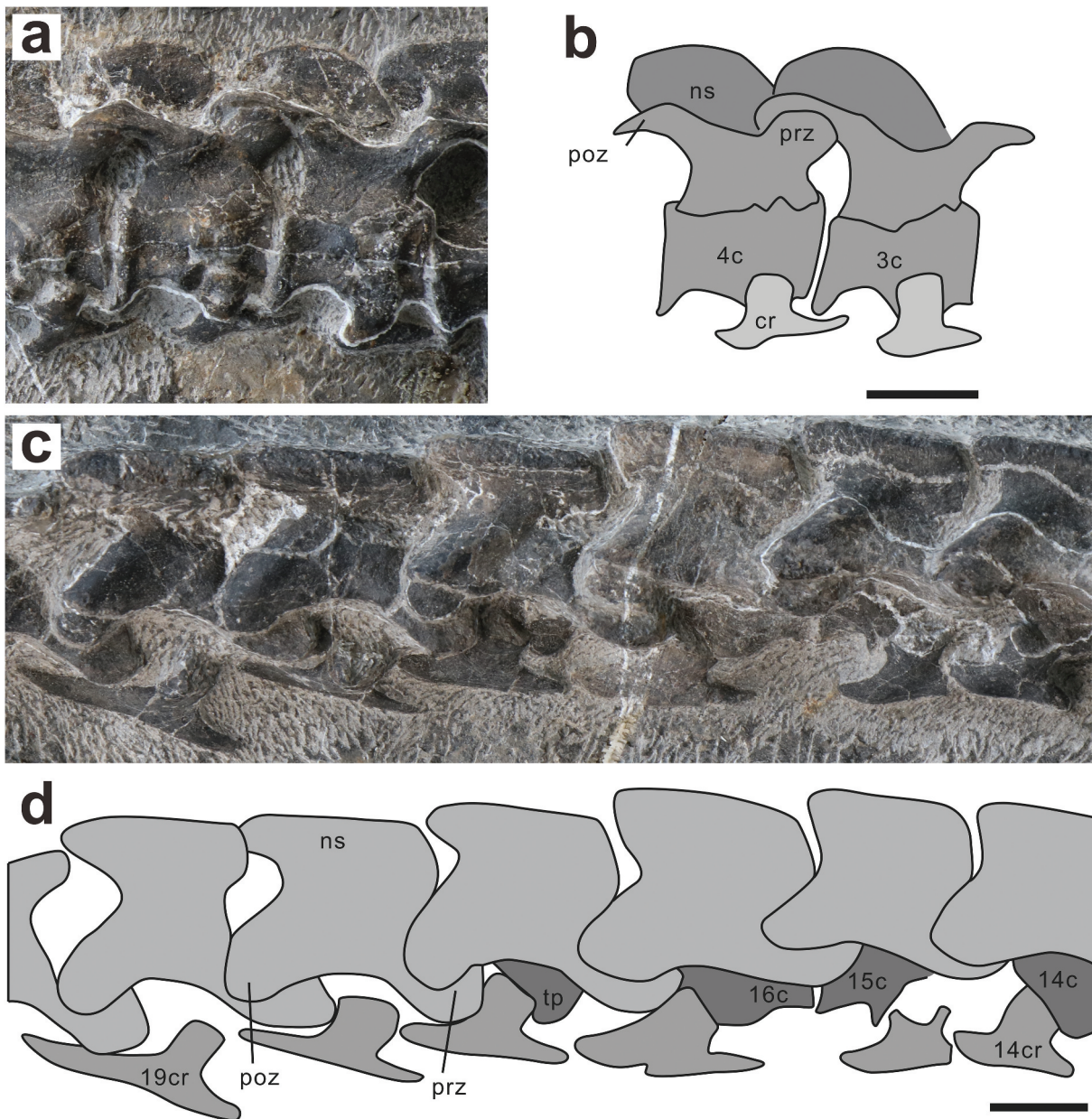


**Figure 4.** The anterior process of cervical ribs of HFUT-LX-19-001. (a) Photo showing 3<sup>rd</sup> and 4<sup>th</sup> cervical vertebra; (b) Interpretative drawing of (a); (c) Photo showing 14<sup>th</sup>-19<sup>th</sup> cervical vertebra; (d) Interpretative drawing of (c). Abbreviations: c, cervical centrum; cr, cervical rib; ns, neural spine; poz, postzygapophysis; prz, prezygapophysis; tp, transverse process. Scale bars equal 1 cm.

end of the trough in HFUT LX-19-001. Finally, there are five dentary fangs in HFUT LX-19-001, rather than four as in *N. youngi*.

In summary, HFUT LX-19-001 differs from the four other nothosaurid species from the Middle Triassic of South China in the unique combination of following characters: jugal positioned more forward in the cheek, pineal foramen located close to the middle of the skull table and towards the anterior end of a deep trough, and distinctly long internal naris. Considering the incomplete nature of HFUT LX-19-001, we refrain from naming a new taxon here, awaiting the discovery of more complete specimens from the region.

#### Morphological comparison of the lower jaw between HFUT LX-19-001 and other Triassic eosauroptrygians

The medial morphology of the lower jaw of eosauroptrygians is scanty. Among nothosaurid sauropterygians, only the

posterior part of the lower jaw of *Nothosaurus mirabilis* (Rieppel 1994) is briefly figured. In addition, *Simosaurus gaillardotii* (Rieppel 1994), *Anarosaurus heterodontus* (Klein 2009), *Neusticosaurus pusillus* (Sander 1989), and *Yunguisaurus liae* (Sato et al. 2010; Stubbs and Benton 2016) among other Triassic eosauroptrygians provide some clue to the medial morphology of the lower jaw (Figure 7). Here, we compare the medial morphology of the lower jaw of HFUT LX-19-001 with that of other Triassic eosauroptrygians, aiming to reveal new informative morphological characters that may be used for constructing a solid phylogenetic relationship of eosauroptrygians in the future.

Dentary – In medial view, the exposed area of the dentary in HFUT LX-19-001 is smaller than in other eosauroptrygians. In *S. gaillardotii*, the dentary forms the most of the anterior medial wall of the lower jaw.

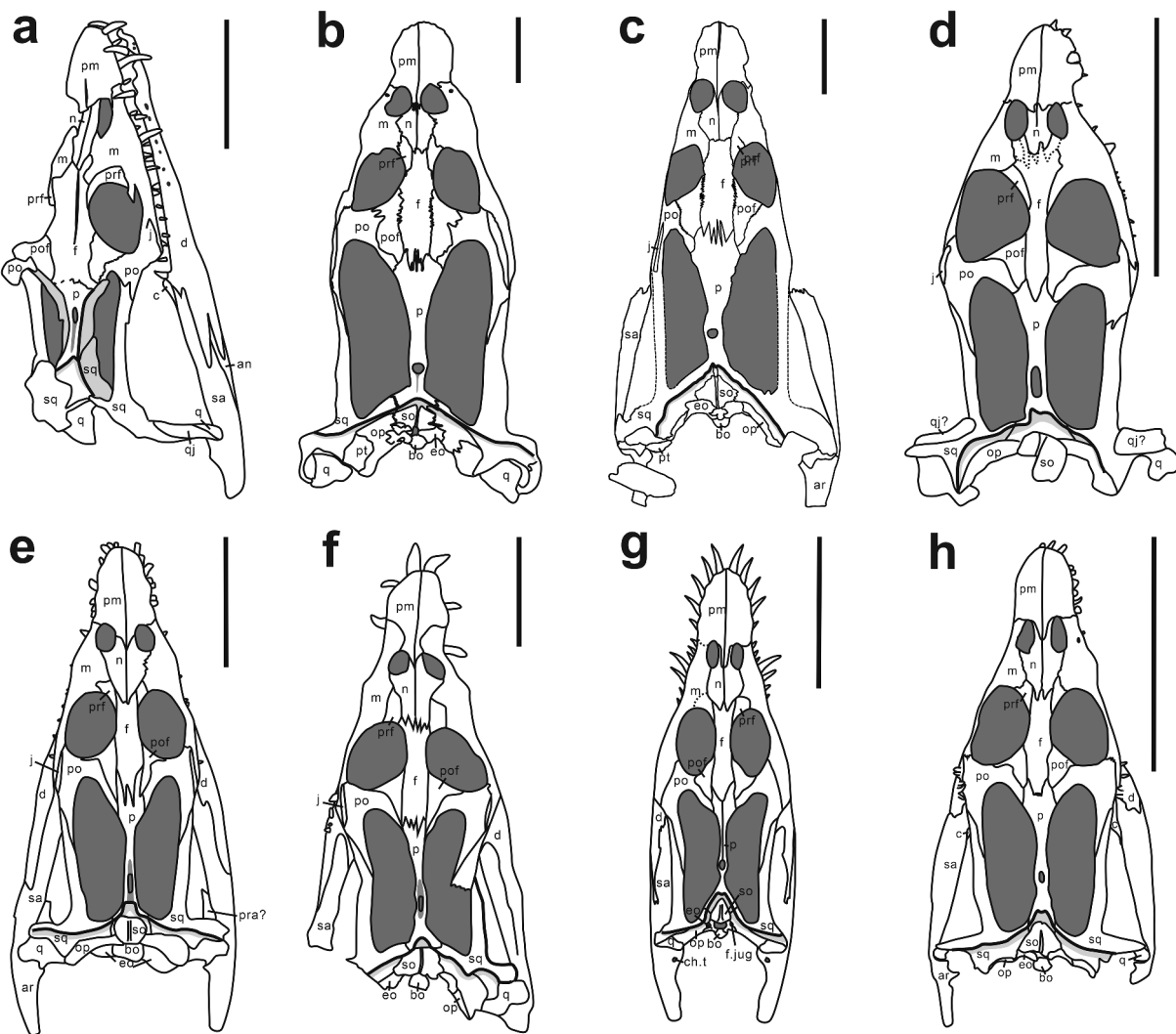


**Figure 5.** The dorsal view of the skull of nothosauroids from the Middle Triassic of South China. (a) HFUT LX-19-001; (b) *N. yangjuanensis* (holotype: GMPKU-P-1080; modified from Jiang et al. 2006a); (c) *N. yangjuanensis* (GMPKU-P-3014; modified from Yin et al. 2014); (d) *L. hongguoensis* (holotype: GMPKU-P-1011; modified from Jiang et al. 2006b); (e) *N. youngi* (holotype: IVPP V 13590; modified from Li and Rieppel 2004); (f) *N. youngi* (WS-30-R24; modified from Ji et al. 2014); (g) Reconstruction of *L. xingyiensis* (holotype: IVPP V 11866; modified from Rieppel et al. 2003) (h) *L. xingyiensis* (XNGM WS-30-R19; modified from Lin et al. 2017). Abbreviations: an, angular; ar, articular; bo, basioccipital; c, coronoid; ch.t, chorda tympani foramen; d, dentary; eo, exoccipital; f, frontal; f. jug, jugular foramen; j, jugal; m, maxilla; n, nasal; op, opisthotic; p, parietal; pm, premaxilla; po, postorbital; pof, postfrontal; prf, prefrontal; q, quadrate; qj, quadratojugal; sa, surangular; so, supraoccipital; sq, squamosal. Scale bars equal 5 cm.

**Splenial** – Compared with *S. gaillardotii* and *Neusticosaurus pusillus*, the splenial is a large element in HFUT LX-19-001. In HFUT LX-19-001, the posterior process of the splenial, with a concave margin, is separated from the surangular by the coronoid. This is similar to *S. gaillardotii*. But in *N. mirabilis* and *Neusticosaurus pusillus*, the splenial runs back at a level between the surangular and prearticular.

**Angular** – In *S. gaillardotii* and *Y. liae*, the exposed angular is larger in medial view than that in HFUT LX-19-001. In *Neusticosaurus pusillus*, the angular is absent in medial view.

**Surangular** – The surangular of HFUT LX-19-001 is larger than that of *Neusticosaurus pusillus* and *S. gaillardotii*, where the surangular only forms one-third of the posterior medial wall of the lower jaw. *N. mirabilis* shares a similarly sized surangular with HFUT LX-19-001.

**Coronoid** – HFUT LX-19-001 and *Neusticosaurus pusillus* are similar in having an elongated coronoid in medial view. But the coronoid of the former runs into the splenial, while the latter enters between the dentary and splenial. *Simosaurus gaillardotii* has a small

triangular coronoid. The coronoid of *Yunguisaurus liae* (Sato et al. 2010) is the largest among the above mentioned taxa if the identification is correct.

**Prearticular** – In HFUT LX-19-001, the anterior process of the prearticular runs into the coronoid and splenial, as in *Simosaurus gaillardotii*. This is different from *Neusticosaurus pusillus* where the prearticular is separated from the coronoid. But the prearticular extends backward to form the bottom and lateral wall of the adductor fossa and retroarticular process in HFUT LX-19-001, as in *Nothosaurus mirabilis*, but being different from *S. gaillardotii*.

**Meckelian foramen** – The Meckelian foramen (or Meckelian fossa) opens on the medial wall of the lower jaw. Except for the exiting vein from the lower jaw, among the three separate trigeminal nerve branches, one of them, named the mandibular nerve (CN V<sub>3</sub>), goes into the mandibular through the Meckelian foramen and meets the facial nerve here (Romer 1956; Benton and Westoll 1983). The mandibular nerve carries both sensory and muscle motor stimuli of the lower jaw. This foramen can only be observed in HFUT LX-19-001 and *N. mirabilis* among Triassic

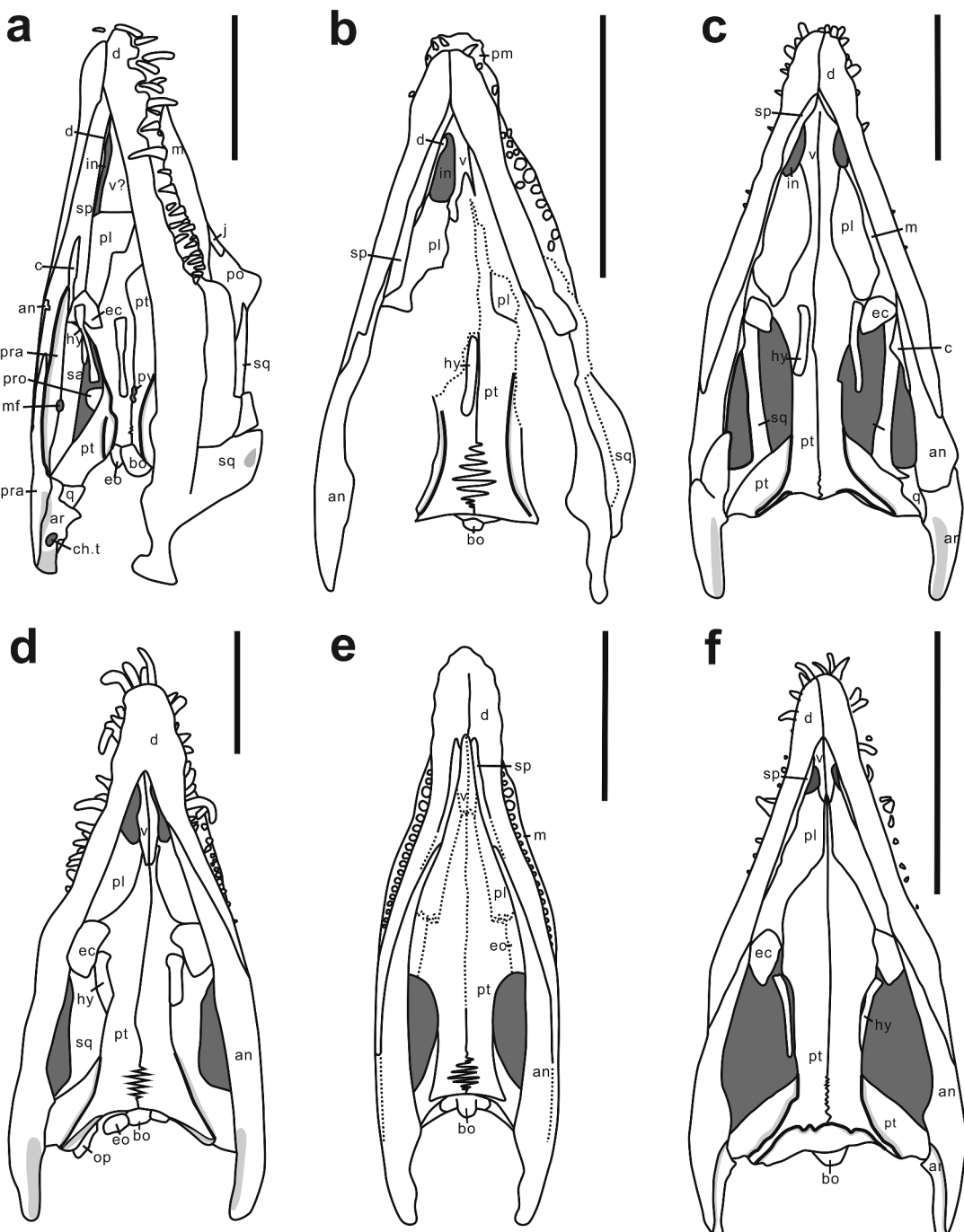


**Figure 6.** The ventral view of the skull of nothosaurids from the Middle Triassic of South China. (a) HFUT LX-19-001; (b) *L. hongguoensis* (holotype: GMPKU-P-1011; modified from Jiang et al. 2006b); (c) *N. youngi* (holotype: IVPP V 13590; modified from Li and Rieppel 2004); (d) *N. youngi* (WS-30-R24; modified from Ji et al. 2014); (e) Reconstruction of *L. xingyiensis* (holotype: IVPP V 11866; modified from Rieppel et al. 2003); (f) *L. xingyiensis* (XNGM WS-30-R19; modified from Lin et al. 2017). Abbreviations: an, angular; ar, articular; bo, basioccipital; c, coronoid; ch.t, chorda tympani foramen; d, dentary; ec, ectopterygoid; eo, exoccipital; hy, hyoid; j, jugal; in, internal naris; m, maxilla; mf, Meckelian foramen; op, opisthotic; pl, palatine; pm, premaxilla; po, postorbital; pra, prearticular; pro, prootic; pt, pterygoid; pv, palatine vacuity; q, quadrate; sa, surangular; sp, splenial; sq, squamosal; v, vomer. Scale bars equal 5 cm.

eosauroppterygians. In HFUT LX-19-001, this foramen is bounded by the surangular and prearticular. In *N. mirabilis*, there is a foramen in nearly the same position, but it is not described by Rieppel (1994). In *S. gaillardotii*, the Meckelian groove is only exposed in front of the splenial. In the holotype of *Y. liae*, the Meckelian canal is exposed at the posterior part of the lower jaw. It is embraced by the coronoid dorsally and angular ventrally (Sato et al. 2010). In the typical reptilian mandible, the Meckelian foramen is located in front of the adductor fossa (Romer 1956). Thus,

the position of the Meckelian foramen as shown by both HFUT LX-19-001 and *N. mirabilis* may be an autapomorphy of Nothosauridae.

#### Phylogenetic implication

Detailed comparison with other Triassic eosauroppterygians reveals that HFUT LX-19-001 represents a new morphotype of nothosaurid sauropterygians from the Middle Triassic of South China.

**Table 2.** Cranial proportions of HFUT LX-19-001 compared with other nothosaurids from the Middle Triassic of South China (*N. youngi*, *N. yangjuanensis*, *L. hongguoensis*, *L. xingyiensis*).

Nothosaurids	HFUT LX-19-001	<i>N. yangjuanensis</i>		<i>L. hongguoensis</i>		<i>N. youngi</i>		<i>L. xingyiensis</i>	
		GMPKU-P-1080	GMPKU-P-3014	GMPKU-P-1011	IVPP V 13590	WS-30-R24	IVPP V 11866	XNGM WS-30-R19	
Cranial proportions									
Condyllobasal skull length/distance from tip to the anterior margin of the external naris	5.77	6.00	6.80	5.92	5.52	4.84	5.11	5.51	
Distance from posterior margin of external naris to anterior margin of orbit/width of the postorbital arch	2.32	1.29	1.57	1.85	2.14	2.39	2.02	2.38	
Longitudinal diameter of temporal fenestra/longitudinal diameter of orbit	1.50	2.55	2.38	1.42	2.04	1.96	1.91	1.69	
Longitudinal diameter of upper temporal fenestra/longitudinal diameter of external naris	3.24	5.96	4.67	3.47	5.00	4.69	5.14	3.67	

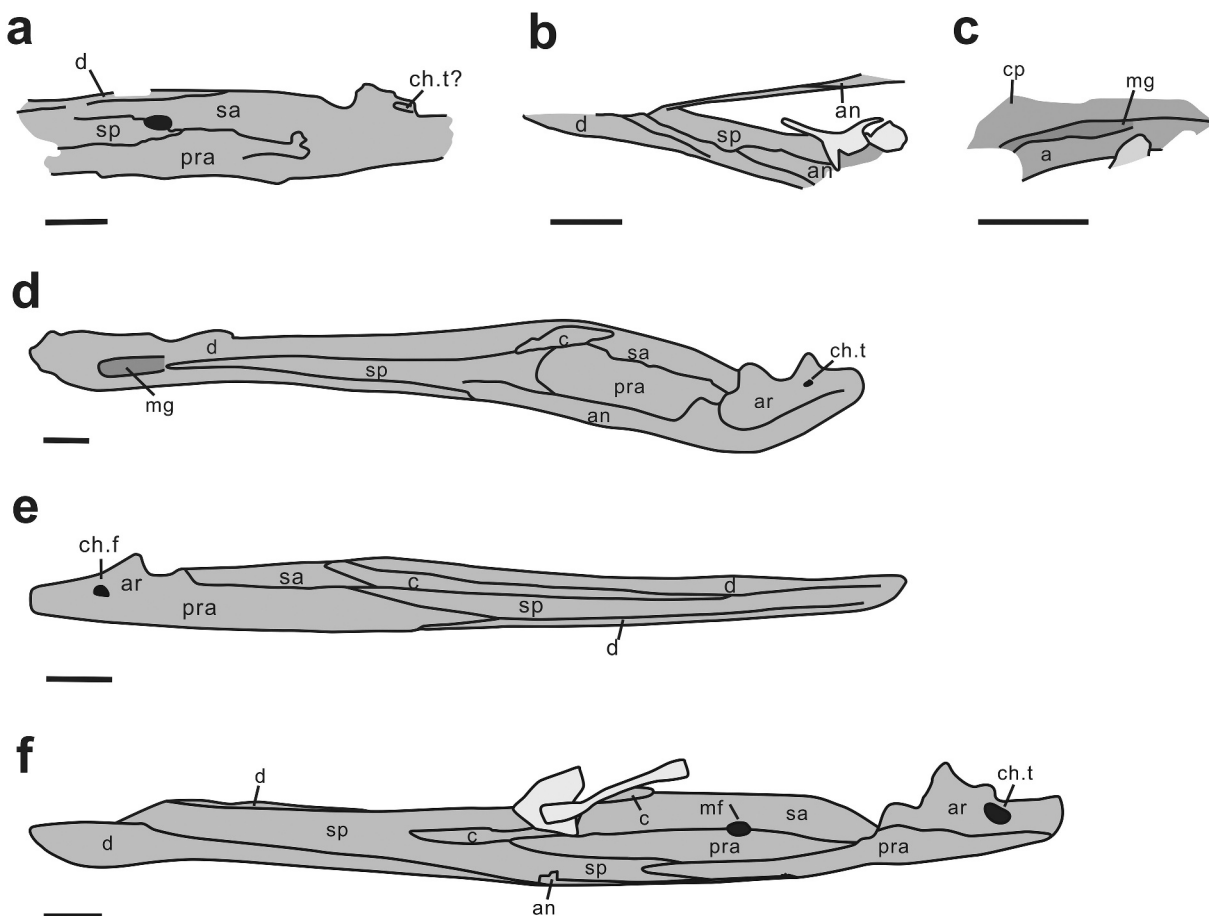


**Figure 7** The medial view of the lower jaw in different Triassic eosaurophterygians. (a) *Nothosaurus mirabilis* (SMNS 59818; modified from Rieppel 1994); (b) *Yunguisaurus liae* (IVPP V14993; modified from Shang et al. 2017); (c) *Yunguisaurus liae* (NMNS 004529/F003862, the holotype; modified from Sato et al. 2010); (d) *Simosaurus gaillardotii* (SMNS 16638; modified from Rieppel 1994); (e) *Neusticosaurus pusillus* (reconstruction; modified from Sander 1989); (f) HFUT LX-19-001. Abbreviations: an, angular; ar, articular; c, coronoid; ch.f, chorda tympani foramen; cp, coronoid process; d, dentary; mf, meckelian foramen; mg, Meckelian groove; pra, prearticular; sa, surangular; sp, splenial. Scale bars equal 2 cm.

HFUT LX-19-001 is also one of few eosaurophterygians showing the medial morphology of the lower jaw. The recent phylogenetic analyses focusing on the interrelationship of nothosaurid species reveal the inadequacy of phylogenetically informative characters used in the data matrix (Liu et al. 2014; Klein et al. 2016; Li and Liu 2020; Lin et al. 2021). Comparison with other Triassic eosaurophterygians (Figure 7) provides new informative morphological characters that may be used for constructing a solid phylogenetic relationship of eosaurophterygians in the future. These new characters include the exposed size of the dentary in medial view, the

exposed size and shape of the splenial in medial view, the exposed size of the angular in medial view, the exposed size of the surangular in medial view, the exposed size and shape of the coronoid in medial view, the contact between the coronoid and prearticular, and the position of the Meckelian foramen.

#### Acknowledgments

We thank L.Y. Li and T. Sato for preparing the specimen, S.P. Jiang and other members from the Paleontological Lab of HFUT for the help in the field, A.S.

Wolniewicz and Q. Li for the discussion of the specimen, D.Y. Jiang, Q.H. Shang, C. Li and F. Zheng for the specimen access, and two anonymous reviewers for helpful comments. This work was supported by the National Natural Science Foundation of China under Grant numbers 42172026 and 41772003, the Fundamental Research Funds for the Central Universities of China under Grant number PA2020GDKC0022, and the Department of Natural Resources of Anhui Province under Grant number 2021-g-2-16.

## Disclosure statement

No potential conflict of interest was reported by the author(s).

## Funding

This work was supported by the National Natural Science Foundation of China [41772003, 42172026]; Department of Natural Resources of Anhui Province [2021-g-2-16]; Fundamental Research Funds for the Central Universities of China [PA2020GDKC0022].

## ORCID

Jun Liu  <http://orcid.org/0000-0001-7859-5209>

## References

- Baur G. 1889. *Palaeohatteria* Credner, and the Proganosauria. Am J Sci. 37:310–313.
- Benson RBJ, Butler RJ, Lindgren J, Smith AS. 2010. Mesozoic marine tetrapod diversity: mass extinctions and temporal heterogeneity in geological mega-biases affecting vertebrates. Proceedings of the Royal Society B: Biological Sciences. 277(1683):829–834. doi:[10.1098/rspb.2009.1845](https://doi.org/10.1098/rspb.2009.1845).
- Benton MJ, Westoll TS. 1983. The Triassic reptile *Hyperodapedon* from Elgin: functional morphology and relationships. Philos. Trans. R. Soc. B: Biol. Sci. 302(1112):605–718.
- Benton MJ, Zhang Q, Hu S, Chen ZQ, Wen W, Liu J, Huang J, Zhou C, Xie T, Tong J, et al. 2013. Exceptional vertebrate biotas from the Triassic of China, and the expansion of marine ecosystems after the Permo-Triassic mass extinction. Earth-Sci Rev. 125:199–243. doi:[10.1016/j.earscirev.2013.05.014](https://doi.org/10.1016/j.earscirev.2013.05.014).
- Hinz JK, Matzke AT, Pfretzschner HU. 2019. A new nothosaur (Sauropterygia) from the Ladinian of Vellberg-eschenau, southern Germany. J Vertebr Paleontol e1585364. 39(2):e1585364. doi:[10.1080/02724634.2019.1585364](https://doi.org/10.1080/02724634.2019.1585364).
- Jiang DY, Maisch MW, Hao WC, Sun YL, Sun ZY. 2006b. *Nothosaurus yangtzeensis* n. sp (Reptilia, Sauropterygia, Nothosauridae) from the middle Anisian (Middle Triassic) of Guizhou, southwestern China. Neues Jahrb Geol Paläontol Abh. 2006(5):257–276. doi:[10.1127/njgpm/2006/2006/257](https://doi.org/10.1127/njgpm/2006/2006/257).
- Jiang DY, Maisch MW, Sun ZY, Sun YL, Hao WC. 2006a. A new species of *Lariosaurus* (Reptilia, Sauropterygia) from the middle Anisian (Middle Triassic) of southwestern China. Neues Jahrb Geol Palaontol Abh. 242 (1):19–42. doi:[10.1127/njgpa/242/2006/19](https://doi.org/10.1127/njgpa/242/2006/19).
- Ji C, Jiang DY, Rieppel O, Motani R, Tintori A, Sun ZY. 2014. A new specimen of *Nothosaurus youngi* from the Middle Triassic of Guizhou, China. J Vertebr Paleontol. 34(2):465–470. doi:[10.1080/02724634.2013.808204](https://doi.org/10.1080/02724634.2013.808204).
- Kelley NP, Pyenson ND. 2015. Evolutionary innovation and ecology in marine tetrapods from the t-Triassic to the Anthropocene. Science. 348(6232):aaa3716. doi:[10.1126/science.aaa3716](https://doi.org/10.1126/science.aaa3716).
- Klein N. 2009. Skull morphology of *Anarosaurus heterodontus* (Reptilia: Sauropterygia: Pachypleurosauria) from the Lower Muschelkalk of the Germanic Basin (Winterswijk, the Netherlands). J Vertebr Paleontol. 29 (3):665–676. doi:[10.1671/039.029.0327](https://doi.org/10.1671/039.029.0327).
- Klein N, Dfae V, Haarhuis A, Bleeker R. 2016. The earliest record of the genus *Lariosaurus* from the early middle Anisian (Middle Triassic) of the Germanic Basin. J Vertebr Paleontol. 36(4):e1163712. doi:[10.1080/02724634.2016.1163712](https://doi.org/10.1080/02724634.2016.1163712).
- Li Q, Liu J. 2020. An Early Triassic sauropterygian and associated fauna from South China provide insights into t-Triassic ecosystem health. Commun. Biol. 3(1):63. doi:[10.1038/s42003-020-0778-7](https://doi.org/10.1038/s42003-020-0778-7).
- Li JL, Liu J, Rieppel O. 2002. A new species of *Lariosaurus* (Sauropterygia: Nothosauridae) from Triassic of Guizhou, southwest China. Vert. PalAs. 40 (2):114–126.
- Lin WB, Jiang DY, Rieppel O, Motani R, Ji C, Tintori A, Sun ZY, Zhou M. 2017. A new specimen of *Lariosaurus xingyiensis* (Reptilia, Sauropterygia) from the Ladinian (Middle Triassic) Zhuganpo Member, Falang formation, Guizhou, China. J Vertebr Paleontol. 37(2):e1278703. doi:[10.1080/02724634.2017.1278703](https://doi.org/10.1080/02724634.2017.1278703).
- Lin W, Jiang D, Rieppel O, Motani R, Tintori A, Sun Z, Zhou M. 2021. *Panzhousaurus rotundirostris* Jiang et al., 2019 (Diapsida: Sauropterygia) and the recovery of the monophyly of Pachypleurosauridae. J Vertebr Paleontol. 41(1). doi:[10.1080/02724634.2021.1901730](https://doi.org/10.1080/02724634.2021.1901730).
- Li JL, Rieppel O. 2004. A new nothosaur from Middle Triassic of Guizhou, China. Vert PalAs. 42(1):1–12.
- Lin J, Hu SX, Rieppel O, Jiang DY, Benton MJ, Kelley NP, Aitchison JC, Zhou CY, Wen W, J-y H, et al. 2014. A gigantic nothosaur (Reptilia: Sauropterygia) from the Middle Triassic of SW China and its implication for the Triassic biotic recovery. Sci Rep. 4(1):1–9. doi:[10.1038/srep07142](https://doi.org/10.1038/srep07142).
- Liu XQ, Lin WB, Rieppel O, Sun ZY, Li ZG, Lu H, Jiang DY. 2015. A new specimen of *Diandongosaurus acutidentatus* (Sauropterygia) from the Middle Triassic of Yunnan, China. Vert PalAs. 53(4):281–290.
- Meyer H. 184755. Die Saurier des Muschelkalkes mit Rücksicht auf die Saurier aus buntem Sandstein und Keuper. Zur Fauna der Vorwelt. 2:1–167.
- Motani R. 2009. The evolution of marine reptiles. Evol.: Educ. Outreach. 2 (2):224–235.
- Motani R, Jiang DY, Rieppel O, Xue YF, Tintori A. 2015. Adult sex ratio, sexual dimorphism and sexual selection in a Mesozoic reptile. Proceedings of the Royal Society B: Biological Sciences. 282(1815):20151658. doi:[10.1098/rspb.2015.1658](https://doi.org/10.1098/rspb.2015.1658).
- Motani R, Vermeij GJ. 2021. Ecophysiological steps of marine adaptation in extant and extinct non-avian tetrapods. Biol Rev. 96(5):1769–1798. doi:[10.1111/brv.12724](https://doi.org/10.1111/brv.12724).
- Owen R. 1860. Palaeontology; or, a Systematic Summary of Extinct Animals and Their Geologic Remains. Edinburgh: Adam and Charles Black.
- Rieppel O. 1994. Osteology of *Simosaurus gailliardotii* and the relationships of stem-group Sauropterygia. Fieldiana (Geology) Ns. 28:1–85.
- Rieppel O, editor. 2000. Sauropterygia I. Vol. 12A. Munich: Verlag Dr. Friedrich Pfeil. Encyclopedia of Paleoherpetology.
- Rieppel O, Li JL, Jun L. 2003. *Lariosaurus xingyiensis* (Reptilia: Sauropterygia) from the Triassic of China. Can J Earth Sci. 40(4):621–634. doi:[10.1139/e02-067](https://doi.org/10.1139/e02-067).
- Rieppel O, Sander PM, Storrs GW. 2002. The skull of the pistosauro *Augustasaurus* from the Middle Triassic of northwestern Nevada. J Vertebr Paleontol. 22(3):577–592. doi:[10.1671/0272-4634\(2002\)022\[0577:TSOTP\]2.0.CO;2](https://doi.org/10.1671/0272-4634(2002)022[0577:TSOTP]2.0.CO;2).
- Romer A. 1956. Osteology of the Reptiles. Chicago and London: The University of Chicago Press.
- Sander PM. 1989. The pachypleurosaurids (Reptilia: Nothosauria) from the Middle Triassic of Monte San Giorgio (Switzerland) with the description of a new species. Philos Trans R Soc Lond B Biol Sci. 325 (1230):561–666.
- Sander PM, Griebeler EM, Klein N, Juarbe JV, Wintrich T, Revell LJ, Schmitz L. 2021. Early giant reveals faster evolution of large body size in ichthyosaurs than in cetaceans. Science. 374(6575):eabf5787. doi:[10.1126/science.abf5787](https://doi.org/10.1126/science.abf5787).
- Sato T, Cheng YN, Wu XC, Li C. 2010. Osteology of *Yunguisaurus* Cheng et al., 2006 (Reptilia; Sauropterygia), a Triassic pistosauroid from China. Paleontol Res. 14(3):179–195. doi:[10.2517/1342-8144.14.3.179](https://doi.org/10.2517/1342-8144.14.3.179).
- Sato T, Zhao LJ, Wu XC, Li C. 2014. *Diandongosaurus acutidentatus* Shang, Wu & Li, 2011 (Diapsida: Sauropterygia) and the relationships of Chinese eosauroptrygians. Geol Mag. 151(1):121–133. doi:[10.1017/S0016756813000356](https://doi.org/10.1017/S0016756813000356).
- Scheyer TM, Romano C, Jenks J, Bucher H. 2014. Early Triassic marine biotic recovery: the predators' perspective. PLoS ONE. 9(3):e88987. doi:[10.1371/journal.pone.0088987](https://doi.org/10.1371/journal.pone.0088987).
- Shang QH. 2006. A new species of *Nothosaurus* from the early Middle Triassic of Guizhou, China. Vert PalAs. 44(3):237–249.
- Shang QH, Sato T, Li C, Wu XC. 2017. New osteological information from a 'juvenile' specimen of *Yunguisaurus* (Sauropterygia; Pistosauroidea). Palaeoworld. 26(3):500–509. doi:[10.1016/j.palwor.2016.05.008](https://doi.org/10.1016/j.palwor.2016.05.008).
- Stubbs TL, Benton MJ. 2016. Ecomorphological diversifications of Mesozoic marine reptiles: the roles of ecological opportunity and extinction. Paleobiology. 42(4):547–573. doi:[10.1017/pab.2016.15](https://doi.org/10.1017/pab.2016.15).
- YBGMR (Yunnan Bureau of Geology and Mineral Resources). 1990. Regional Geology of Yunnan Province. Beijing: Geological Publishing House.
- Yin C, Hao W, Sun Z, Sun Y, Jiang D. 2014. New material of *Nothosaurus yangtzeensis* from the middle Anisian (Middle Triassic) of Guizhou Province, Southwestern China. Acta Scientiarum Naturalium Universitatis Pekinensis. 50(3):467–475.